Polarization of Lyman-α Line Due to the Anisotropy of Electron Collisions in a Plasma

symmetry

MDPI

Article

Polarization of Lyman-α Line Due to the Anisotropy of Electron Collisions in a Plasma

Motoshi Goto [1,2,*] and Nilam Ramaiya [3]

[1] National Institute for Fusion Science, Toki 509-5292, Japan
[2] Department of Fusion Science, The Graduate University for Advanced Studies, SOKENDAI, Toki 509-5292, Japan
[3] Institute for Plasma Research, Gandhinagar 382428, India; nilam@ipr.res.in
* Correspondence: goto.motoshi@nifs.ac.jp

Abstract: We have developed an atomic model for calculating the polarization state of the Lyman-α line in plasma caused by anisotropic electron collision excitations. The model assumes a nonequilibrium state of the electron temperature between the directions parallel ($T_{\parallel}$) and perpendicular ($T_{\perp}$) to the magnetic field. A simplified assumption on the formation of an excited state population in the model is justified by detailed analysis of population flows regarding the upper state of the Lyman-α transition with the help of collisional-radiative model calculations. Calculation results give the polarization degree of several percent under typical conditions in the edge region of a magnetically confined fusion plasma. It is also found that the relaxation of polarization due to collisional averaging among the magnetic sublevels is effective in the electron density region considered. An analysis of the experimental data measured in the Large Helical Device gives $T_{\perp}/T_{\parallel} = 7.6$ at the expected Lyman-α emission location outside the confined region. The result is derived with the absolute polarization degree of 0.033, and $T_{\perp} = 32\,\mathrm{eV}$ and $n_e = 9.6 \times 10^{18}\,\mathrm{m}^{-3}$ measured by the Thomson scattering diagnostic system.

Keywords: plasma spectroscopy; polarization; Lyman-alpha; nuclear fusion

Citation: Goto, M.; Ramaiya, N. Polarization of Lyman-α Line Due to the Anisotropy of Electron Collisions in a Plasma. *Symmetry* **2021**, *13*, 297. https://doi.org/10.3390/sym13020297

Academic Editor: Eugene Oks
Received: 22 January 2021
Accepted: 5 February 2021
Published: 9 February 2021

1. Introduction

In a magnetically confined fusion plasma, the velocity distribution function (VDF) of electrons and ions is thought to be more or less anisotropic. For example, energetic ions are unidirectionally introduced by the neutral beam, and the cyclotron motions of ions and electrons are selectively accelerated by the electron cyclotron resonance heating (ECRH) and the ion cyclotron resonance heating (ICRH), respectively. Because of the unavoidable magnetic field ripple, confinement characteristics are different between the particles having a large pitch angle and a small pitch angle with respect to the magnetic field. The former and the latter are called trapped particles and passing particles, respectively, and are sometimes treated separately when the particle transport is considered.

An example of the research relating to this topic is the influence of plasma pressure anisotropy on the MHD (Magnetohydrodynamic) equilibria, which has been intensively investigated [1]. The ITER experiment would also be influenced by the problem of anisotropy [2]. In the Large Helical Device (LHD), the so-called density clamping observed with strong ECRH is thought to be attributed to the difference in the confinement characteristics of the trapped and passing electrons [3]. The anisotropy also plays a role in the plasma edge region. The radial electric field formation in the edge stochastic region is thought to be related to the anisotropy in the electron VDF (EVDF) [4].

Although the anisotropy is regarded as an important subject for characterizing the plasma confinement as seen above, no reliable measurement method for the anisotropic VDF of electrons and ions has been established to date. Under such circumstances, polarization spectroscopy has been proposed as a technique to address the problem of anisotropy

in the EVDF [5]. This novel diagnostic method consists of two issues, i.e., the measurement of polarization in line emission from the plasma and the construction of an atomic model for analyzing the observation data. A critical problem in the measurement is a difficulty in detecting the polarization of line emission with accuracy, the degree of which is estimated in the order of one percent or smaller. Although some measurements have been attempted, no reliable results have been obtained [6,7].

Recently, the CLASP (Chromospheric Lyman-Alpha SpectroPolarimetry) project led by the NAOJ (National Astronomical Observatory of Japan) has successfully measured the polarization state of the hydrogen Lyman-α line in the solar atmosphere [8]. Although the polarization formation mechanism in the solar atmosphere is photoexcitation by the anisotropic radiation field, which is different from the mechanism in the fusion plasma, the observation technique itself can be transferred to the measurement for a fusion plasma. Actually, the same technique as CLASP has been attempted in LHD, and the polarization of the Lyman-α line has been successfully detected [9].

As for the atomic model, a sophisticated framework has been developed by Fujimoto [5], and some actual applications have been made [6,10]. We here report details of the implementation of Fujimoto's framework for the Lyman-α line with goal of utilizing it for the analysis of the polarization data taken in the LHD experiment. Furthermore, an analysis has been made of the LHD experimental data and derivation of an anisotropic EVDF is attempted.

2. Theoretical Model for the Line Emission Polarization

2.1. Polarization Formation of the Lyman-α Line

The polarization of an emission line originates in a population imbalance between the magnetic sublevels in the upper state of the transition. The Lyman-α line consists of two fine structure lines, i.e., $1\,^2S_{1/2}-2\,^2P_{1/2}$ and $1\,^2S_{1/2}-2\,^2P_{3/2}$. Figure 1 shows all transitions between magnetic sublevels composing the Lyman-α line. The $\Delta m_J = 0$ and $\Delta m_J = \pm 1$ transitions emit light linearly polarized in the quantization axis direction (π light) and circularly polarized on the plane perpendicular to the quantization axis (σ light), respectively, where m_J is the magnetic quantum number. The numbers next to the lines indicating the transitions are the relative values of the Einstein A coefficients. It is confirmed that if all the magnetic sublevels have the same population, the intensities of π, σ^+, and σ^- lights are identical, i.e., there is no polarization, and otherwise the line is polarized.

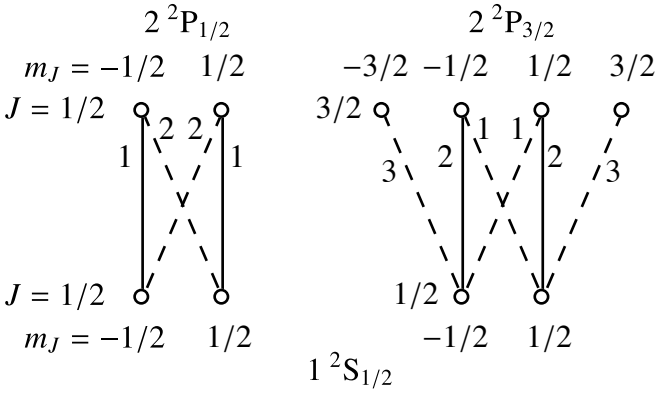

Figure 1. Line components included in the Lyman-α line. The solid and dashed lines represent the π- and σ-light, respectively. The numbers next to the lines indicate relative values of the Einstein A coefficient.

We assume axisymmetry with respect to the quantization axis which is taken in the magnetic field direction later. In this case, the population distribution has a "mirror symmetry", i.e., the populations of m_J and $-m_J$ sublevels are identical in each of the $2\,^2P_{1/2}$ and $2\,^2P_{3/2}$ states. Because of this restriction, the line corresponding to the $1\,^2S_{1/2}-2\,^2P_{1/2}$

transition is never polarized because π, σ^+, and σ^- light intensities are always identical. As for the $1\,^2S_{1/2}-2\,^2P_{3/2}$ transition, populations of the $m_J = |1/2|$ and $m_J = |3/2|$ substates in the $2\,^2P_{3/2}$ state can be different, which could give rise to the line polarization because only the $m_J = |1/2|$ substates are responsible for the π light. We first focus on deriving the polarization state of the $1\,^2S_{1/2}-2\,^2P_{3/2}$ line and then incorporate the influence of the unpolarized $1\,^2S_{1/2}-2\,^2P_{1/2}$ line into the result as explained below to enable a direct comparison of the model results with the observation results.

When the measurement is made from the direction perpendicular to the quantization axis with a linear polarizer, the polarization degree P of an emission line is generally defined as

$$P = \frac{I_\pi - I_\sigma}{I_\pi + I_\sigma}, \tag{1}$$

where I_π and I_σ represent the line intensities observed when the polarizer is directed in the direction parallel and perpendicular to the quantization axis, respectively. Because the Lyman-α line includes the two fine structure components, P can be explicitly written as

$$P = \frac{(I_\pi(3/2) + I_\pi(1/2)) - (I_\sigma(3/2) + I_\sigma(1/2))}{(I_\pi(3/2) + I_\pi(1/2)) + (I_\sigma(3/2) + I_\sigma(1/2))}, \tag{2}$$

where $I_\pi(1/2)$ and $I_\sigma(1/2)$ are the intensities of the π- and σ-components of the $1\,^2S_{1/2}-2\,^2P_{1/2}$ line, respectively, and $I_\pi(3/2)$ and $I_\sigma(3/2)$ are the same but of the $1\,^2S_{1/2}-2\,^2P_{3/2}$ line, respectively. Because the $1\,^2S_{1/2}-2\,^2P_{1/2}$ line is unpolarized under the present condition, the relation

$$I_\pi(1/2) - I_\sigma(1/2) = 0 \tag{3}$$

should always hold. On the other hand, we assume that the population ratio of the $2\,^2P_{1/2}$ state to the $2\,^2P_{3/2}$ state follows the ratio of their statistical weights, i.e., the former is half the latter. In that case, the same is true for the line intensities of the $1\,^2S_{1/2}-2\,^2P_{1/2}$ and $1\,^2S_{1/2}-2\,^2P_{3/2}$ transitions, i.e.,

$$I_\pi(1/2) + I_\sigma(1/2) = \frac{1}{2}[I_\pi(3/2) + I_\sigma(3/2)]. \tag{4}$$

By using the relations of Equations (3) and (4), we can rewrite Equation (2) as

$$\begin{aligned} P &= \frac{(I_\pi(3/2) - I_\sigma(3/2)) + (I_\pi(1/2) - I_\sigma(1/2))}{(I_\pi(3/2) + I_\sigma(3/2)) + (I_\pi(1/2) + I_\sigma(1/2))} \\ &= \frac{I_\pi(3/2) - I_\sigma(3/2)}{\frac{3}{2}[I_\pi(3/2) + I_\sigma(3/2)]} \\ &= \frac{2}{3}P(3/2), \end{aligned} \tag{5}$$

where $P(3/2)$ is the polarization degree of the $1\,^2S_{1/2}-2\,^2P_{3/2}$ line.

2.2. Polarization Due to Anisotropic Electron Collisions

The condition of an excited state which has a population imbalance among the magnetic sublevels is well represented by the density matrix [11]. Under an axisymmetric system, the spherical coordinate representation of the density matrix ρ of the state $2\,^2P_{3/2}$ can be expanded [5] as

$$\rho(p) = \rho_0^0(p)T_0^{(0)}(p) + \rho_0^2(p)T_0^{(2)}(p), \tag{6}$$

where p stands for the state $2\,^2P_{3/2}$ and $T_q^{(k)}(p)$ is the so-called irreducible tensor operator. The coefficients $\rho_0^0(p)$ and $\rho_0^2(p)$ respectively correspond to the population and the alignment, the latter of which expresses the inhomogeneity over the magnetic sublevels in the state p. We hereafter use $a(p)$ instead of $\rho_0^2(p)$ for simplicity. The conventional population

is given as $n(p) = \sqrt{2J+1}\rho^0_0(p)$, where J is the total angular momentum quantum number of the state p.

The population imbalance among the magnetic sublevels could be created by anisotropic electron collisions. We consider a simple atomic model for a quantitative calculation of $n(p)$ and $a(p)$ where the population inflow and outflow concerning the state p are balanced by the electron impact excitation of the ground state atoms and the spontaneous radiative decay. Such a condition can be expressed [5] as

$$C^{0,0}(1,p)n_{\mathrm{e}}n(1) = \sum_s A(p,s)n(p), \tag{7}$$

where $C^{0,0}(1,p)$ is the rate coefficient of the electron impact excitation from the ground state denoted as "1" to the state p, $A(p,s)$ is the Einstein A coefficient of the transition from p to a state s placed energetically lower than p, and n_{e} is the electron density. The validity of this model under the conditions assumed here will be examined later.

The equilibrium condition of $a(p)$ is similarly expressed [5] as

$$C^{0,2}(1,p)n_{\mathrm{e}}n(1) = \left[\sum_s A(p,s) + C^{2,2}(p,p)n_{\mathrm{e}}\right]a(p), \tag{8}$$

where $C^{0,2}(1,p)$ is the alignment creation rate coefficient accompanying the excitation from the ground state to the state p and $C^{2,2}(p,p)$ is the alignment destruction rate coefficient in the state p. The population $n(p)$ and the alignment $a(p)$ are then expressed as

$$n(p) = \frac{C^{0,0}(1,p)n_{\mathrm{e}}}{\sum_s A(p,s)}n(1), \tag{9}$$

$$a(p) = \frac{C^{0,2}(1,p)n_{\mathrm{e}}}{\sum_s A(p,s) + C^{2,2}(p,p)n_{\mathrm{e}}}n(1). \tag{10}$$

As discussed in Section 2.1, the measurement gives the polarization degree P. We here introduce another quantity, "longitudinal alignment", A_{L}, which is defined slightly differently from P [5] as

$$\begin{aligned} A_{\mathrm{L}} &= \frac{I_\pi - I_\sigma}{I_\pi + 2I_\sigma} \\ &= \frac{2P}{3-P}. \end{aligned} \tag{11}$$

The longitudinal alignment for the transition from the state p to s, i.e., $A_{\mathrm{L}}(p,s)$, is directly related to $a(p)/n(p)$, the normalized alignment, [5] as

$$A_{\mathrm{L}}(p,s) = (-1)^{J_p+J_s}\sqrt{\frac{3}{2}}(2J_p+1)\begin{Bmatrix} J_p & J_p & 2 \\ 1 & 1 & J_s \end{Bmatrix}\frac{a(p)}{n(p)}, \tag{12}$$

where $\{\cdots\}$ is the 6-j symbol, and J_p and J_s are the total angular momentum quantum numbers of the states p and s, respectively.

Calculations of the coefficients $C^{0,0}(1,p)$ and $C^{0,2}(1,p)$ can be carried out under a certain EVDF. We assume that the EVDF is axisymmetric with respect to the quantization axis and is expressed by two temperatures, $T_\parallel$ and $T_\perp$, which are in the directions parallel and perpendicular, respectively, to the quantization axis (or the magnetic field). Such EVDFs are explicitly given [5] as

$$f(v,\theta) = \left(\frac{m}{2\pi k}\right)^{3/2}\left(\frac{1}{T_\perp^2 T_\parallel}\right)^{1/2}\exp\left[-\frac{mv^2}{2k}\left(\frac{\sin^2\theta}{T_\perp} + \frac{\cos^2\theta}{T_\parallel}\right)\right], \tag{13}$$

where v is the absolute velocity, θ is the pitch angle of the velocity with respect to the quantization axis, and m and k are the electron mass and the Boltzmann constant, respectively. The function $f(v,\theta)$ is here normalized as

$$2\pi \iint f(v,\theta) v^2 \sin\theta \mathrm{d}v\mathrm{d}\theta = 1. \tag{14}$$

Figure 2 shows examples of $f(v,\theta)$ in the case of $T_\perp = 30\,\mathrm{eV}$ and $T_\parallel = 10\,\mathrm{eV}$ (a) and of $T_\perp = 30\,\mathrm{eV}$ and $T_\parallel = 100\,\mathrm{eV}$ (b). It is noted that when we focus our interest on a group of electrons having any constant absolute velocity, the number of electrons is larger in the higher temperature direction than in the lower temperature direction.

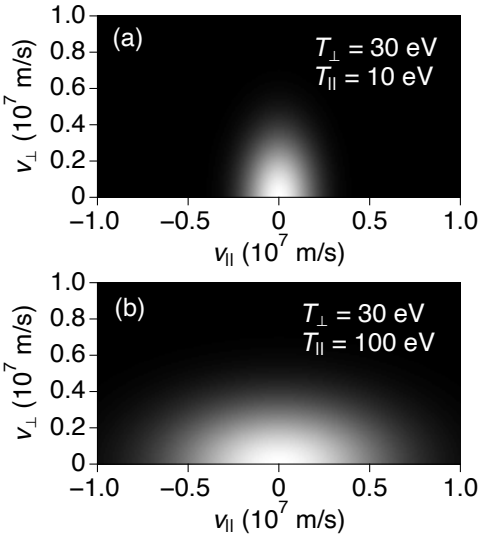

Figure 2. Examples of the electron velocity distribution function $f(v,\theta)$ for (**a**) $T_\perp = 30\,\mathrm{eV}$ and $T_\parallel = 10\,\mathrm{eV}$, and (**b**) $T_\perp = 30\,\mathrm{eV}$ and $T_\parallel = 100\,\mathrm{eV}$ cases.

The rate coefficients $C^{0,0}(1,p)$ and $C^{0,2}(1,p)$ are calculated [5] as

$$C^{0,0}(1,p) = \int Q_0^{0,0}(1,p) 4\pi f_0(v) v^3 \mathrm{d}v \tag{15}$$

and

$$C^{0,2}(1,p) = \int Q_0^{0,2}(1,p) [4\pi f_2(v)/5] v^3 \mathrm{d}v, \tag{16}$$

respectively, where $Q_0^{0,0}(1,p)$ and $Q_0^{0,2}(1,p)$ are the excitation and alignment creation cross sections, respectively, for the excitation from the ground state to the state p, and $f_0(v)$ and $f_2(v)$ are the coefficients of the expansion of $f(v,\theta)$ by the Legendre polynomials $P_K(\cos\theta)$ as

$$f(v,\theta) = \sum_K f_K(v) P_K(\cos\theta). \tag{17}$$

The coefficient $f_K(v)$ is explicitly given as

$$f_K(v) = \frac{2K+1}{2} \int f(v,\theta) P_K(\cos\theta) \sin\theta \, \mathrm{d}\theta. \tag{18}$$

The alignment creation cross section $Q_0^{0,2}(1,p)$ is derived from $Q_0^{0,0}(1,p)$ as [5].

$$Q_0^{0,2}(1,p) = (-1)^{J_p+J_s} \sqrt{\frac{2}{3}} (2J_p+1)^{-1} \left\{ \begin{array}{ccc} J_p & J_p & 2 \\ 1 & 1 & J_s \end{array} \right\}^{-1} A_{\mathrm{L}}(p,1) Q_0^{0,0}(1,p), \tag{19}$$

with A_L for the case when the excitation takes place with mono-energetic beam collisions. We adopt the cross section data by Bray [12] for $Q_0^{0,0}$ and by James [13] for P which is translated into A_L by Equation (11). It is noted that the data found in Refences [12,13] include both the $1\,^2S_{1/2}-2\,^2P_{1/2}$ and $1\,^2S_{1/2}-2\,^2P_{3/2}$ transitions. We here assume that 2/3 of the total cross section is for the $1\,^2S_{1/2}-2\,^2P_{3/2}$ transition, and the total polarization degree multiplied by 3/2 is for the $1\,^2S_{1/2}-2\,^2P_{3/2}$ transition (cf. Equation (5)). Figure 3 shows these elemental quantities relating to the $1\,^2S_{1/2}-2\,^2P_{3/2}$ transition. The opposite polarity between A_L and $Q_0^{0,2}$ is due to the 6-j symbol which is negative in the present case.

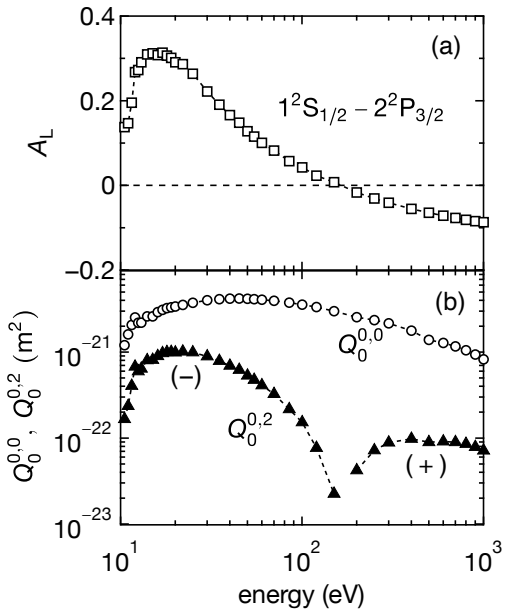

Figure 3. A_L values under an assumption of a mono-energetic beam collision experiment (**a**) and $Q_0^{0,0}$ and $Q_0^{0,2}$ (**b**) for the $1\,^2S_{1/2}-2\,^2P_{3/2}$ transition. The actual $Q_0^{0,2}$ labeled with $(-)$ takes negative values.

The alignment destruction process is understood as the relaxation of the population imbalance among the magnetic sublevels. It is known that this process due to electron collisions has some correlation with the Stark broadening of the emission line from that state and its rate coefficient can be approximated by the half width of the Stark broadening [14]. Here, the Stark broadening data for the Lyman-α line by Stehlé [15] are adopted for evaluating $C^{2,2}(p,p)n_e$. The results are plotted in Figure 4. It is confirmed that the alignment destruction rate increases almost linearly with n_e.

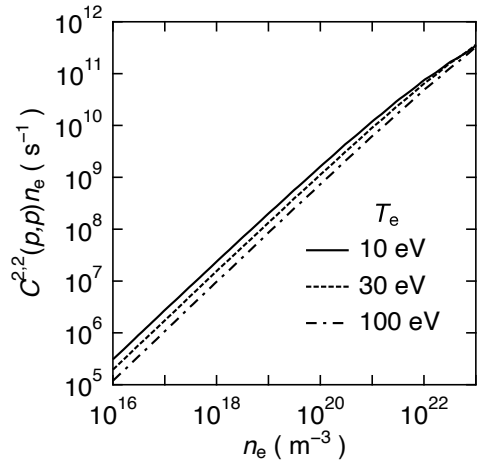

Figure 4. Alignment destruction rate $C^{2,2}(p,p)n_e$ evaluated from the Stark broadening width [15].

3. Results and Discussion

We have calculated A_L for the Lyman-α line for typical plasma conditions in LHD as an example. The quantization axis is taken in the direction of the magnetic field. In our previous experimental study, we found that the linearly polarized light intensity takes on a maximum (minimum) value in the direction perpendicular (parallel) to the magnetic field [9]. Therefore, it is natural to regard the magnetic field direction as the symmetry axis of the system. The calculation is made with $T_\perp$ fixed at 32 eV, where the experimental data analyzed later are borne in mind, while $T_\parallel$ is scanned in a range around the fixed $T_\perp$. We adopt several n_e values which cover a typical n_e range for the edge region of a magnetic fusion plasma. The polarization degree P for the Lyman-α line is derived from the A_L values with Equation (11), and the results are plotted in Figure 5.

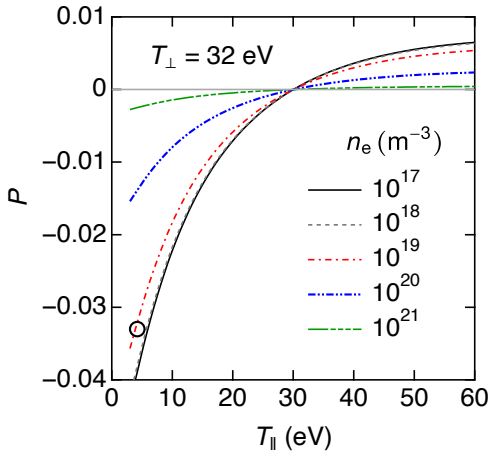

Figure 5. Example of the calculation results for P with several n_e values. $T_\perp$ is fixed at 32 eV and $T_\parallel$ is scanned. The open circle represents the combination of $n_e = 9.6 \times 10^{19}$ m^{-3} and $P = -0.033$ corresponding to the experimental value in Ref. [9], from which $T_\parallel = 4.2$ eV is derived.

It is confirmed that the line is unpolarized when $T_\parallel = T_\perp$, and the absolute polarization degree decreases with increasing n_e, which is caused by collisional averaging over the magnetic sublevels. The positive P values for $T_\parallel > T_\perp$ indicate that the π-light intensity is larger than that of σ-light, and negative P values for $T_\parallel < T_\perp$ mean the opposite condition. These results are inferred from the tendency of the elemental P data in Figure 3 as follows.

In the present T_e range at around 30 eV, the collision energy lower than 100 eV is dominant, and such collisions give rise to a positive A_L or P as seen in Figure 3a. A positive A_L or P means a higher intensity of linearly polarized light in the direction parallel with the electron beam axis than in the perpendicular direction (cf. Equation (1)). The condition of $T_\perp > T_\parallel$ means more electrons in the perpendicular direction than in the direction parallel to the magnetic field as seen in Figure 2, which causes a higher intensity in the perpendicular direction than in the direction parallel to the magnetic field. This tendency finally results in a negative A_L or P. The negative P values in the case of $T_\parallel < T_\perp$ can be understood similarly.

We have recently reported a value of $P = -0.033$ as an example in the actual measurement in LHD where the quantization axis is taken in the magnetic field direction [9]. In LHD, it is known that the radial location of neutral hydrogen emissions is almost fixed irrespective of the plasma condition [16–18], and local T_e and n_e at the emission location are obtained from the radial T_e and n_e profiles measured by the Thomson scattering diagnostic system. In the experiment where $P = -0.033$ is obtained, the T_e and n_e at the Lyman-α emission location are found to be 32 eV and 9.6×10^{18} m^{-3}, respectively. Because the Thomson scattering diagnostic system for LHD measures light scattered by electrons moving predominantly in the direction perpendicular to the magnetic field, this T_e value can be regarded as $T_\perp$ in our model calculation. We now have $T_\perp$ and n_e at the emission location

as well as P. Figure 5 indicates that $T_{\parallel}$ can be determined when $T_{\perp}$ and n_e are known so as to give the measured P. In the present case, $T_{\parallel} = 4.2\,\mathrm{eV}$ is derived.

The atomic model developed in Section 2 assumes a simple mechanism for the formation of the excited level population. Here, the validity of the present model is examined with a collisional-radiative model (CR-model) for atomic hydrogen [19] which treats energy levels resolved only by the principal quantum number p.

The CR-model solves coupled rate equations for all of the excited levels considered in the model under the quasi-steady-state condition [19] for determining the population distribution over the excited levels. Because the present plasma is in the ionizing state [20], each excited level population is expressed as

$$n(p) = R_1(p) n_e n(1), \tag{20}$$

where $R_1(p)$ is called the population coefficient of the level p and is a function of n_e and T_e, and $n(1)$ stands for the ground state density. The CR-model derives $R_1(p)$ for all the excited levels considered.

By using the results of the CR-model, we have evaluated breakdowns of the population flows from and to the $p = 2$ level. Figure 6a shows the n_e dependence of component fractions of the inflow to the $p = 2$ level from other levels at $T_e = 10\,\mathrm{eV}$. It is found that more than 90% of the inflow is dominated by the electron impact excitation, and the cascades from higher levels account for the remaining part of the inflow in the n_e range of our interest, i.e., from $10^{18}\,\mathrm{m}^{-3}$ to $10^{19}\,\mathrm{m}^{-3}$. We have confirmed that the results are hardly changed at $T_e = 30\,\mathrm{eV}$. This result justifies the assumption regarding the populating process of the $p = 2$ level in the present model in Section 2.

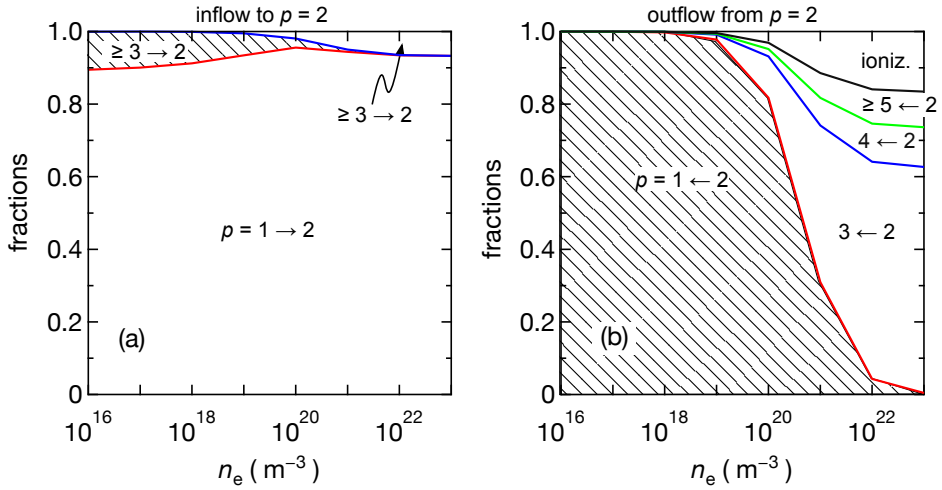

Figure 6. Fractions of breakdowns for the (**a**) population inflow to the level $p = 2$ and (**b**) population outflow from the level $p = 2$ as a function of n_e at $T_e = 10\,\mathrm{eV}$. The numbers represent the principal quantum number of the levels and the arrows indicate the transition direction. The hatched and open areas indicate the radiative and collisional transitions, respectively. The label "ioniz". means the ionization.

Similar results concerning the outflow from the $p = 2$ are shown in Figure 6b. It is found that the radiative decay to the ground state predominates over other processes in the n_e range of our interest, which supports the assumption for the depopulating process from the $p = 2$ level in the model. Because collisional transition rates between different l-levels and j-levels are generally small as compared to those between p-levels under the conditions assumed here [21,22], the present model is regarded as a good approximation for the plasma considered.

In this paper, we have developed an atomic model for analyzing polarization states of the Lyman-α line where observations of the magnetically confined fusion plasma are

borne in mind. The simplified model adopted is confirmed to be adequate through analyses for the populating mechanism of the $p = 2$ level which is the upper state of the Lyman-α line emission. An analysis of experimental data has been attempted with the present model, and the anisotropy is derived in terms of the difference in T_e between the magnetic field direction and the direction perpendicular to it. It is finally noted that the model developed in this paper is dedicated to the Lyman-α line, and therefore the anisotropy can be diagnosed in the limited narrow region where the Lyman-α line emission mainly takes place. However, the methodology can be easily transferred to other emission lines of other atoms and ions, so that an appropriate emission line can be chosen depending on the plasma region where the interest is focused.

Author Contributions: Conceptualization, methodology, and writing, M.G.; formal analysis, N.R.; investigation, M.G. and N.R. All authors have read and agreed to the published version of the manuscript.

Funding: This research was partly supported by JSPS KAKENHI Grant Number 18K03588 and by the National Institute for Fusion Science grant administrative budgets (ULHH028).

Acknowledgments: We thank Takashi Fujimoto for his helpful suggestions concerning the collisional process of polarization relaxation.

Conflicts of Interest: The authors declare no conflict of interest. The funders had no role in the design of the study; in the collection, analyses, or interpretation of data; in the writing of the manuscript, or in the decision to publish the results.

references

1. Qu, Z.S.; Fitzgerald, M; Hole, M.J. Analysing the impact of anisotropy pressure on tokamak equilibria. *Plasma Phys. Contr. Fusion* **2014**, *56*, 075007. [CrossRef]
2. Hole, M. J.; Qu, Z.; Pinches, S.; Schneider, M.; Arbina, I.L.; Mantsinen, M.J.; Sauter, O. The impact of anisotropy on ITER scenarios. *Nucl. Fusion* **2020**, *60*, 112010. [CrossRef]
3. Makino, T. Local and Fast Density Pump-out by ECRH in the LHD. *Plasma Fusion Res.* **2013**, *8*, 2402115. [CrossRef]
4. Rozhansky, V. Drifts, Currents, and Radial Electric Field in the Edge Plasma with Impact on Pedestal, Divertor Asymmetry and RMP Consequences. *Contrib. Plasma Phys.* **2014**, *54*, 508–-516. [CrossRef]
5. Fujimoto, T. Population-Alignment Collisional-Radiative Model. In *Plasma Polarization Spectroscopy*; Fujimoto, T., Iwamae, A., Eds.; Springer: Berlin, Germany, 2008; pp. 51–68.
6. Fujimoto, T.; Sahara, H.; Kawachi, T.; Kallstenius, T.; Goto, M.; Kawase, H.; Terumichi, Y. Polarization of impurity emission lines from a tokamak plasma. *Phys. Rev. E* **1996**, *54*, R2240–R2243. [CrossRef]
7. Herzog, O.; Weinheimer, J.; Rosmej, F.B.; Kunze, H.J.; Bertschinger, G.; Bitter, M.; Urnov, A. The Bragg-polarimeter at TEXTOR 94. In Proceedings of the Japan-US Workshop on Plasma Polarization Spectroscopy and The International Seminar on Plasma Polarization Spectroscopy, NIFS-PROC-37, Kyoto, Japan, 26–28 January 1998; pp. 33–38.
8. Kano, R.; Bueno, J.T.; Winebarger, A.; Auchère, F.; Narukage, N.; Ishikawa, R.; Carlsson, M. Discovery of Scattering Polarization in the Hydrogen Lyα Line of the Solar Disk Radiation. *ApJL* **2017**, *839*, L10. [CrossRef]
9. Ramaiya, N.; Goto, M.; Seguineaud, G.; Oishi, T.; Morita, S Measurement of polarization in Lyman-α line caused by anisotropic electron collisions in LHD plasma. *J. Quant. Spectrosc. Radiat. Transf.* **2020**, *260*, 107430. [CrossRef]
10. Iwamae, A.; Sato, T.; Horimoto, Y.; Inoue, K.; Fujimoto, T.; Uchida, M.; Maekawa, T. Anisotropic electron velocity distribution in an ECR helium plasma as determined from polarization of emission lines. *Plasma Phys. Contr. Fusion* **2005**, *47*, L41. [CrossRef]
11. Blum K. *Density Matrix Theory and Applications*, 2nd ed.; Plenum: New York, NY, USA, 1996.
12. Bray, I.; Stelbovics, A.T. Calculation of Electron Scattering on Hydrogenic Targets. *Adv. Atom. Mol. Opt. Phys.* **1995**, *35*, 209–254.
13. James, G.; Slevin, J.A.; Dziczek, D.; McConkey, J.W.; Bray, I. Polarization of Lyman-α radiation from atomic hydrogen excited by electron impact from near threshold to 1800 eV. *Phys. Rev. A Atom. Mol. Opt. Phys.* **1998**, *57*, 1787–1797. [CrossRef]
14. Hirabayashi, A.; Nambu, Y.; Hasuo, M.; Fujimoto, T. Disalignment of excited neon atoms due to electron and ion collisions. *Phys. Rev. A Atom. Mol. Opt. Phys.* **1988**, *37*, 83–88 [CrossRef] [PubMed]
15. Stehlé, C.; Hutcheon, R. Extensive tabulations of Stark broadened hydrogen line profiles. *Astron. Astrophys. Suppl. Ser.* **1999**, *140*, 93–97. [CrossRef]
16. Iwamae, A.; Hayakawa, M.; Atake, M.; Fujimoto, T.; Goto, M.; Morita, S. Polarization resolved H_α spectra from the large helical device: Emission location, temperature, and inward flux of neutral hydrogen. *Phys. Plasmas* **2005**, *12*, 042501. [CrossRef]
17. Iwamae, A.; Sakaue, A.; Neshi, N.; Yanagibayashi, J.; Hasuo, M.; Goto, M.; Morita, S. Hydrogen emission location, temperature and inward velocity in the peripheral helical plasma as observed with plasma polarization spectroscopy. *J. Phys. B: Atom. Mol. Opt. Phys.* **2010**, *43*, 144019. [CrossRef]
18. Goto, M.; Sawada, K. Determination of electron temperature and density at plasma edge in the Large Helical Device with opacity-incorporated helium collisional-radiative model. *J. Quant. Spectrosc. Radiat. Transf.* **2014**, *137*, 23–28. [CrossRef]

19. Sawada, K.; Fujimoto, T. Temporal relaxation of excited-level populations of atoms and ions in a plasma: Validity range of the quasi-steady-state solution of coupled rate equations. *Phys. Rev. E* **1994**, *49*, 5565–5573. [CrossRef] [PubMed]
20. Fujimoto, T. *Plasma Spectroscopy*; Oxford University Press: Oxford, UK, 2004.
21. Hutcheon, R.J.; McWhirter, R.W.P. The intensities of the resonance lines of highly ionized hydrogen-like ions. *J. Phys. B Atom. Mol. Optic. Phys.* **1973**, *6*, 2668–2683. [CrossRef]
22. Zygelman, B.; Dalgarno, A. Impact excitation of the n = 2 fine-structure levels in hydrogenlike ions by protons and electrons. *Phys. Rev. A* **1987**, *35*, 40850–4100. [CrossRef]